Acta Cryst. (1979). A35, 309–314

Defect Structure of the Ionic Conductor Lithium Nitride (Li_3N)

BY HEINZ SCHULZ AND K. H. THIEMANN

Max-Planck-Institut für Festkörperforschung, Heisenbergstrasse 1, *D*-7000 *Stuttgart* 80, *Federal Republic of Germany*

(*Received* 1 *August* 1978; *accepted* 19 *September* 1978)

Abstract

The defect structure of Li_3N (space group *P6/mmm*, $a \simeq 3{\cdot}65$, $c \simeq 3{\cdot}88$ Å) has been investigated with data sets measured at seven temperatures in the range 153 to 678 K. The data have been used for normal and high-order refinements and for the calculation of the corresponding difference electron densities. The final R_w ranged between 0·7 and 1·3%. The N atom position at $z = 0$ and the Li(1) positions at $z = \frac{1}{2}$ are completely occupied and remain ordered within the whole temperature range. The Li(2) sites at $z = 0$ already show a vacancy concentration of 1–2% at low temperatures, which does not change significantly with increasing temperature. The Li(2) ions exhibit strong anharmonic thermal vibrations within the Li_2N layers at $z = 0$ along the Li(2)–Li(2) connection lines. The high Li ionic conduction is caused by jumps of Li(2) ions from an occupied Li(2) site into an unoccupied one. The anharmonic thermal vibrations are the precursors of these jumps. Interstitial sites are not involved in this mechanism.

Introduction

Li_3N crystallizes in space group *P6/mmm*. Its crystal structure (Figs. 1 and 2) can be described as a sequence of Li and Li_2N layers perpendicular to **c**. The N atoms occupy the centre of the elementary cell. They are surrounded by eight Li atoms in the shape of a hexagonal bipyramid. The Li atoms at the apices of this bipyramid form the pure Li layers and the remaining atoms form the Li_2N layers (Zintl & Brauer, 1935; Rabenau & Schulz, 1976).

Low-temperature investigations have shown that Li_3N forms ionic bonds; therefore, its valence formula can be written as $Li_3^+N^{3-}$ (Schulz & Schwarz, 1978; Schwarz & Schulz, 1978). The N^{3-} ion, which is unstable as a free ion, has been found to exist in the solid state for the first time in this compound. Li ions at the Li(1) and Li(2) positions (Figs. 1 and 2) form two and three Li—N bonds with lengths of 1·94 and 2·13 Å respectively. The Li(2) ions are more weakly bonded to the N atoms than the Li(1) ions. This can be seen from the thermal motion (Fig. 2). At both Li positions the thermal-vibration amplitudes are larger perpendicular to the bond directions than parallel to them, with the largest amplitudes observed at the Li(2) positions (Rabenau & Schulz, 1976; Schulz & Schwarz, 1978).

Li_3N shows the highest Li ionic conductivity presently known at ambient and relatively modest temperatures (Boukamp & Huggins, 1976; von Alpen, Rabenau & Talat, 1977).* The ionic conduction is anisotropic: it is larger perpendicular to than parallel to **c** by two orders of magnitude at room temperature. This difference reduces to a factor of five at 570 K (von Alpen, Rabenau & Talat, 1977). From dielectric studies at low temperatures Wahl & Holland (1978) concluded that the ions lie in shallow potential wells.

* Hong (1978) reported that $Li_{14}Zn(GeO_4)_4$ shows a Li ionic conduction comparable to Li_3N in the temperature range 520 to 670 K. However, this material is not stable with respect to pure Li. Its activation energy is higher and its room-temperature conductivity is lower than that of Li_3N (von Alpen, Bell, Wichelhaus, Cheung & Dudley, 1978).

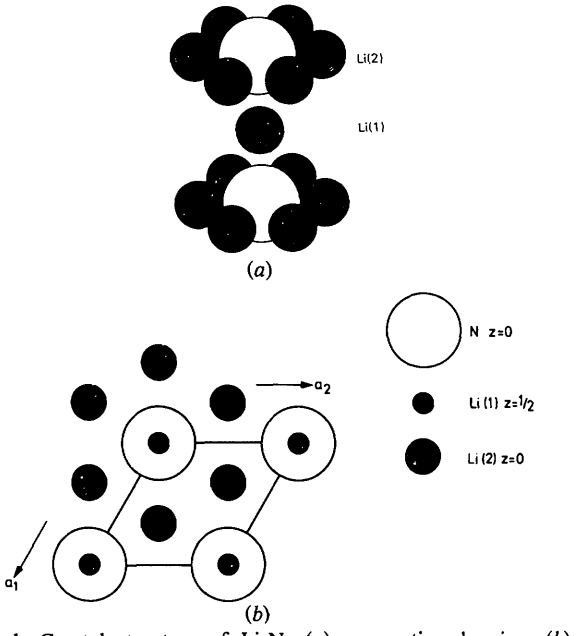

Fig. 1. Crystal structure of Li_3N: (*a*) perspective drawing, (*b*) projection along **c**.

0567-7394/79/020309-06$01.00

The large Li conductivity of Li_3N suggests a high degree of positional Li disorder, as was found, for example, for the Ag ions in α–AgI (Cava, Reidinger & Wuensch, 1977). However, X-ray investigations at room temperature and below (Schulz & Schwarz, 1978) have shown that the Li ions exhibit nearly complete ordering, except that the Li(2) positions have an underoccupation of 1–2%. Related electron density studies did not show residual electron densities outside the atomic positions that could be attributed to these missing Li ions residing in interstitial sites.

The large Li conductivity at room temperature and above and the lack of evidence for Li ions in interstitial sites, as well as the high degree of positional order at room temperature and below, stimulated a detailed investigation of the structural parameters of Li_3N as a function of temperature. These studies are focused on defects within the Li substructure.

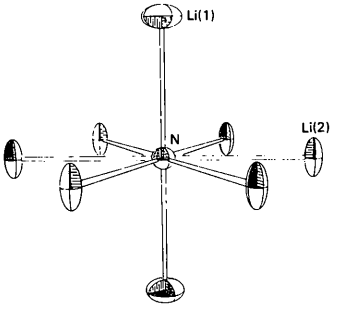

(*a*)

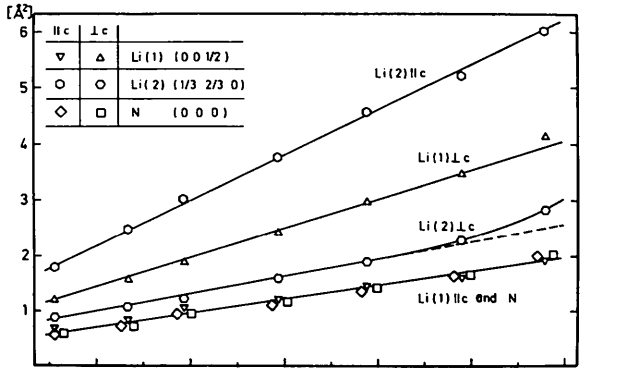

(*b*)

Fig. 2. Thermal motion in Li_3N and coordination polyhedron of the N atoms. (*a*) Thermal-vibration ellipsoids of the Li and N atoms and coordination polyhedron of the N in the form of a hexagonal bipyramid. (*b*) Thermal mean-square displacements u (Å^2) as a function of temperature.

Experimental details

Crystal pieces shaped approximately like a sphere or a cube about 300 μm across were taken from large single crystals grown by the Czochralski technique (Schönherr, Müller & Winkler, 1978). These crystal pieces were put into a tube of Lindemann glass under vacuum. The tube was then filled with dry argon and fused to exclude humidity. The quality of the single crystals prepared in this way was checked by Laue photographs.

Three pieces were selected for measurements on single-crystal diffractometers. The low-temperature measurements (153 to 233 K) were carried out with a Syntex $P2_1$ diffractometer; measurements at higher temperatures were carried out with the Philips PW 1100 equipment.* The crystals were cooled by a nitrogen stream, the temperature being both controlled and measured with an accuracy of ± 10 K. They were heated in a stream of warm air with a temperature precision of ± 2 K. The lattice constants were derived from the angular positions of 14 (Syntex) or 24 reflections (Philips). The intensities were measured in the ω-scan mode up to $\theta = 45°$ and in the $\theta/2\theta$ mode for higher θ values. The intensities of control reflections did not change significantly. Further details of the measurements are listed in Table 1.

Data reduction and structure refinements

Both absorption correction factors and the X-ray path lengths were calculated. The crystal dimensions and shape were determined in place on the diffractometer by optical methods. These measurements were not very accurate because of the presence of the surrounding Lindemann tube. The absorption factors differed from each other by <1% ($\mu = 0{\cdot}064$ mm^{-1} for Mo $K\alpha$ radiation). These correction factors were not applied to the measured intensities because of the low variation among them and the limited accuracy of the crystal-shape measurements; however, the X-ray path lengths were used. The intensities and the corresponding X-ray path lengths were averaged. Weights were calculated from the counting statistics. Further details are listed in Table 1.

* The low-temperature and room-temperature data from the second crystal were utilized earlier (Schulz & Schwarz, 1978).

Table 1. *Details of the intensity measurements and final R values*

T(K)	153	233	293	393	488	588	678
θ(max.) (°)	50	50	50	35	40	40	40
Measured reflections	1188	1188	1188	615	702	702	702
Symmetry-independent reflections	125	125	125	60	82	82	82
R	0·014	0·008	0·012	0·005	0·008	0·009	0·014
$R(w)$	0·013	0·009	0·011	0·009	0·007	0·010	0·013

The structure refinements were carried out as described by Schulz & Schwarz (1978). We used the scattering curves for Li^+ taken from *International Tables for X-ray Crystallography* (1974) and the N^{3-} scattering curves for different stabilizing Watson-sphere potentials (Schwarz & Schulz, 1978). The overall best fit for all data sets was again obtained for the N^{3-} scattering curve calculated with a Watson radius of 1·39 Å. The following ten structure parameters were refined: anisotropic temperature factors (Fig. 2), occupation probabilities of the Li positions (Fig. 4), isotropic extinction correction (Larson, 1967) and scaling factor. For these calculations 60 to 125 symmetrically independent reflections were used (Table 1). The refinements were carried out once with the complete data sets and then with reflections with $\theta > 65°$ for measurements at room temperature and below and $\theta > 30°$ for the high-temperature measurements. The occupation probabilities and temperature factors refined with these two types of data sets agreed within one e.s.d. Naturally, the e.s.d.'s for the high-order refinements were higher than for the refinements with all the data. The results shown in Figs. 2(*b*) and 4 were derived from the complete data sets. The final R values are listed in Table 1.*

Lattice constants, anisotropic temperature factors and occupation probabilities

The lattice constants at different temperatures are shown in Fig. 3: c varies linearly over the whole temperature range. The temperature dependence of a can be described by a straight line only up to 570 K; above this temperature it deviates from this line to higher values.

The thermal-vibration parameters have the form of rotational ellipsoids for all three atomic positions with the main axes oriented parallel to and perpendicular to **c** respectively (Fig. 2*a*).

The following relation holds for harmonic thermal vibrations:

$$u \propto T.Q(\theta/T)/(m_A.\theta^2),$$

where u = mean-square displacement, T = absolute temperature, Q = Debye function, θ = Debye temperature and m_A = atomic mass. Thus the mean-square displacements u are proportional to T. The six symmetrically independent u values in Li_3N follow this relationship up to 570 K. The u ($\perp c$) value of Li(2) deviates from the straight line above 570 K. All other u values follow straight lines up to the highest investigated temperature. The thermal motion of the N atoms can be considered to be isotropic over the whole temperature range, whereas both Li positions exhibit vibrational amplitudes which are larger perpendicular to than in the direction of their bonds (Fig. 2). These results agree with expectations: The environment of the N atoms is nearly isotropic; however, the coordination of the Li atoms [linear for Li(1) and planar for Li(2)] is anisotropic.

The deviation of the u ($\perp c$) component of Li(2) suggests strong anharmonic thermal vibrations of these ions perpendicular to **c** above 570 K.

The linear relationship between u and T also suggests a linear expansion of the lattice constants. This is, however, not true for a at higher temperatures (Fig. 3). The more than linear expansion of a suggests interactions between Li ions. This assumes that Li—Li interactions take place only perpendicular to **c**. This expectation is supported by the results presented in the following section.

The refined occupation probabilities are presented in Fig. 4, which shows that the Li(1) position at $z = \frac{1}{2}$, which forms the pure Li layers (Fig. 1), is completely ordered and remains so at higher temperatures. In contrast, the Li(2) position at $z = 0$ is already underoccupied at low temperatures by about 1–2%. The underoccupation remains nearly constant until 570 K, whereas above this temperature the occupation probability drops, reaching 0·96 at 678 K.

* Lists of structure factors obtained at 153, 233, 293, 393, 588 and 678 K have been deposited with the British Library Lending Division as Supplementary Publication No. SUP 33919 (7 pp.). Copies may be obtained through The Executive Secretary, International Union of Crystallography, 5 Abbey Square, Chester CH1 2HU, England.

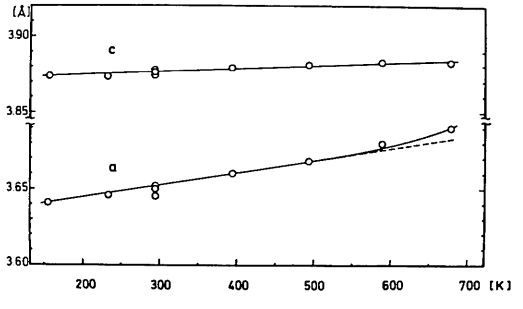

Fig. 3. Lattice constants as a function of temperature.

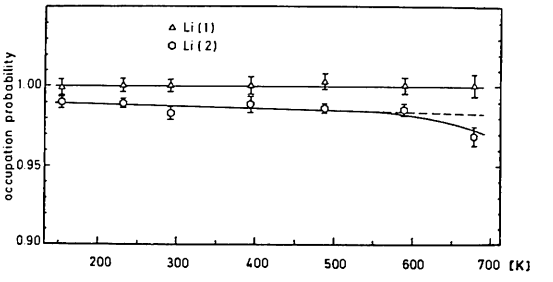

Fig. 4. Occupation probabilities of the Li positions as a functon of temperature.

Difference electron densities and anharmonic thermal vibrations

Difference electron densities (Figs. 5 and 6) were calculated to look for the missing Li(2) ions. Structure parameters determined by a normal least-squares refinement were used for these calculations. The development of the difference electron densities in the Li_2N plane with increasing temperature is shown in Fig. 5(*a*) to (*c*). At 393 K the features around the Li(2) positions suggest anharmonic thermal vibrations of these ions (Fig. 5*a*). One can draw lines from the negative densities to the positive densities through the Li(2) position. The extensions of these lines cross N atom positions at the negative density side and the center between two Li atoms on the positive density side. This effect is already observable at room temperature, as was shown by a similar difference electron density in Fig. 6(*c*) of Schulz & Schwarz (1978). The arrangement of negative and positive densities around the Li(2) ions can be explained by thermal vibration of excited Li(2) ions in the anharmonic part of the Li(2) potential, whereas the remaining ions vibrate in a harmonic or nearly harmonic potential.

The transition of an Li(2) ion from harmonic to anharmonic thermal vibration is illustrated in Fig. 7. The two Li ions in the low and medium excited states both vibrate in a common approximately harmonic potential, whereas the shape of the potential relevant to the Li(2) ion in the highly excited state deviates substantially from that characteristic of harmonic vibrations. Compared to the mean positions of all Li(2) ions at $(\frac{1}{3}, \frac{2}{3}, 0)$ or $(\frac{2}{3}, \frac{1}{3}, 0)$ the highly excited Li(2) ions vibrate with a large amplitude in the direction of the neighboring Li(2) ions and with a small amplitude in the opposite direction, *i.e.* in the direction of the Li(2)—N bonds (Fig. 1). These highly excited Li(2) ions generate positive and negative densities in conventional difference electron densities in the directions of their large and small vibration amplitudes respectively. This distribution of negative and positive densities around the Li(2) positions in Fig. 5 suggests a potential form along the line N—Li(2)—Li(2), such as that shown schematically on the left side of Fig. 7.

This interpretation of the residual densities at 393 K (Fig. 5*a*) is supported by the corresponding electron density map at 588 K (Fig. 5*b*). The positive electron densities around Li(2) are seen to be already connected with each other. Both positive and negative parts are

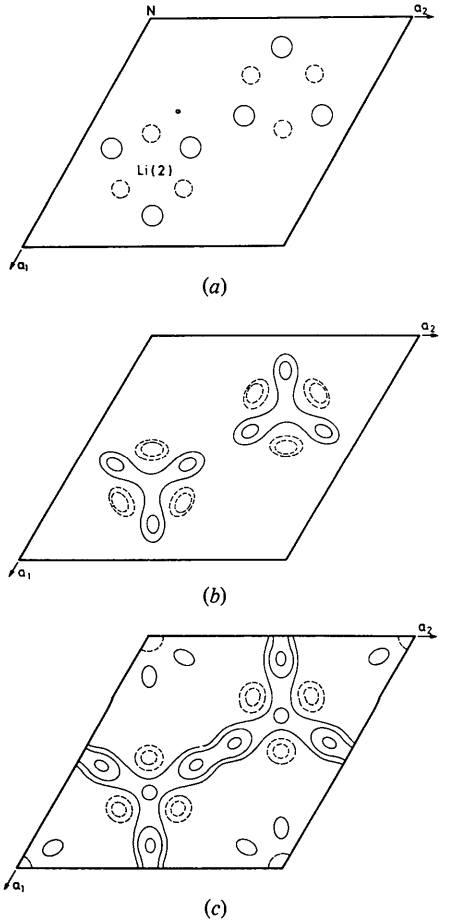

Fig. 5. Difference electron density section through the Li_2N layer at $z = 0$. Full and dotted lines represent positive and negative densities respectively. The lines are drawn at ±0·03, ±0·06, ±0·09 eÅ^{-3}. (*a*) 393 K. (*b*) 588 K. (*c*) 678 K.

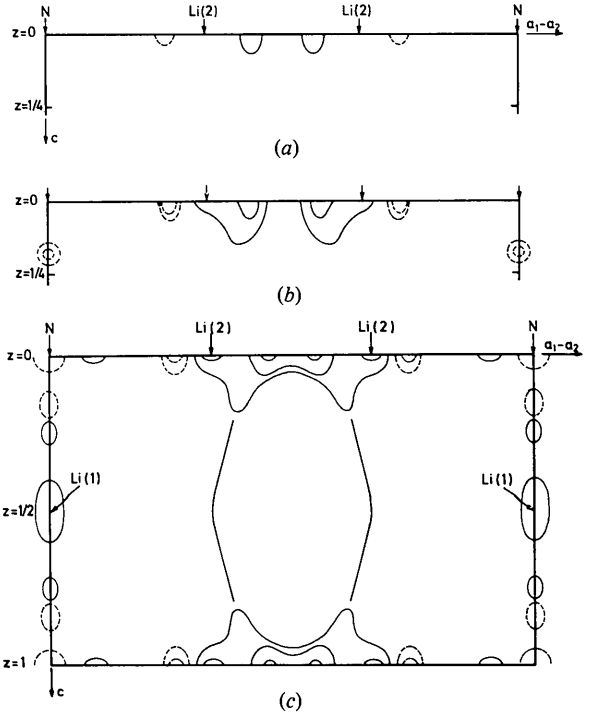

Fig. 6. (*a*)–(*c*) Difference electron density sections along **c** and along the connection line N—Li(2)—Li(2)—N, which coincides with the vector $\mathbf{a}_1-\mathbf{a}_2$. Electron density lines and temperatures are as in Fig. 5.

also expanded compared to those at 393 K (Fig. 5*a*). At 678 K the positive parts have grown together to form a two-dimensional network consistent with the concept of well defined conduction paths for the Li(2) ions. However, the residual electron densities are due to the vibrations of all Li(2) ions in highly excited states, not just those which jump to adjacent sites.

The densities shown in Fig. 5 are limited to the immediate neighborhood of the Li_2N plane at $z = 0$, as shown by the electron density section parallel to **c** (Fig. 6). No densities other than those in Figs. 5 and 6 were found, in any part of the elementary cell, to have either a systematic tendency with temperature or a temperature-independent constant value. Thus it follows that within the limits of this investigation no interstitial sites are observable which can be assigned to the missing Li(2) ions. This was also found for the highest temperature of 678 K, at which the Li(2) position shows a vacancy concentration of about 4%.

Defect structure and ionic conduction mechanism

The results presented in the previous sections lead to the following models of the defect structure and the ionic conduction mechanism in Li_3N.

The Li_3N crystals investigated have a natural vacancy concentration of about 1–2% at the Li(2) positions within the Li_2N layers. This means that about every third elementary cell contains one unoccupied Li(2) site. In contrast, the Li(1) sites are completely occupied. The missing Li(2) ions do not occupy interstitial sites, as there is no evidence that they are incorporated into the crystal. Therefore, the investigated crystals deviate from the exact stoichiometric composition in the direction of a Li deficit. This deviation from complete order may be related to the crystal-growing procedure which may cause an excess of nitrogen in the crystal (Schönherr *et al.*, 1978). Some of the nitrogen may exist as N^{2-} ions. Another assumption is that O^{2-} ions are incorporated into the crystal during the preparation. The charge deficit at N atom sites can then be compensated by vacancies at the Li(2) positions. In this connection it should be taken into account that the Li(2) ions are more weakly bonded to N than the Li(1) ions. Their Li—N distances and their thermal-vibration amplitudes are both significantly larger than those of Li(1) (*cf. Introduction* and Fig. 2).

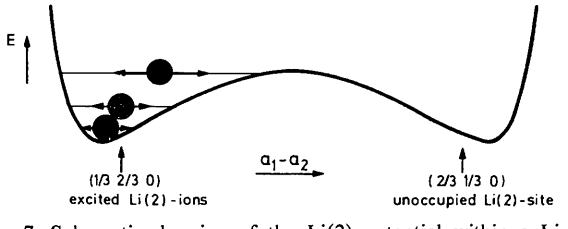

Fig. 7. Schematic drawing of the Li(2) potential within a Li_2N layer ($z = 0$) along the Li(2)–Li(2) connection lines between an occupied and an unoccupied Li(2) site. At the occupied site on the left side three Li(2) ions are shown in low, medium and high excited states.

The vacancy concentration at the Li(2) sites of about 1–2% and the anharmonic thermal vibrations of the Li(2) ions described in the previous section play the most important role in the ionic conduction mechanism of Li_3N. The ionic conduction within the Li_2N layers is undoubtedly related to these anharmonic thermal vibrations. The excited Li(2) ions vibrate along the Li(2)—Li(2) connection lines in a shallow and extended potential (Fig. 7). An excited Li(2) ion needs, therefore, only a small increase in energy to jump into a neighboring unoccupied Li(2) site. Therefore, the ionic conduction perpendicular to **c** takes place predominantly in the Li_2N layers along the Li(2)—Li(2) connection lines. It is a simple vacancy conduction. No interstitial sites seem to be involved in this process.

Ionic conduction parallel to **c** is also related to the anharmonic thermal vibrations of the Li(2) ions. This can be seen from Fig. 6. There are two drop-like extensions of the residual electron density which stick out of the Li_2N plane and which increase in size and height with increasing temperature. The bent lines in Fig. 6(*c*) follow the shape of these drops. The Li(2) ions probably move along these lines from one Li_2N layer to the next. During these movements the Li(2) ions must pass through the positively charged Li(1) layers at $z = \frac{1}{2}$ which therefore form a potential barrier for the jumping Li(2) ions. Therefore, only the most excited Li(2) ions are able to move parallel to **c**. The jump paths of these ions, shown by the bent lines in Fig. 6, all meet at either $(\frac{1}{3},\frac{2}{3},\frac{1}{2})$ or $(\frac{2}{3},\frac{1}{3},\frac{1}{2})$. At these points the jumping Li(2) ions pass through the Li(1) layers at a maximum distance from the Li(1) ions at $(0,0,\frac{1}{2})$. Again Li(2) vacancies rather than interstitials are involved in this process. An Li(2) ion jumps directly from an occupied site to an unoccupied site. There is no evidence that the rather empty Li(1) layers at $z = \frac{1}{2}$ play a role in the ionic conduction either parallel or normal to **c**. This means that these layers do not embody interstitial sites of the Li(2) ions. Furthermore, the Li(1) ions do not contribute to the ionic conduction. Their sites are completely occupied at all investigated temperatures.

The proposed model of the ionic conduction in Li_3N leads to the conclusion that the vacancy mobility is greater perpendicular to **c** than parallel to it. This model explains quite well the observed anisotropic behavior of the ionic conduction (von Alpen *et al.*, 1977). The activation energy has been found to be lower perpendicular to **c** (0·29 eV) than parallel to it (0·49 eV). Furthermore, at room temperature the specific conductivity of Li_3N is two orders of magnitude higher perpendicular to than parallel to **c**. This difference is reduced to a factor of five at 570 K.

Above 570·K the *a* axes (Fig. 3), the mean-square displacement *u* ($\perp c$) of Li(2) (Fig. 2*b*) and the occupation probability of Li(2) (Fig. 4) all deviate from a linear temperature dependence. These deviations are also probably caused by the anharmonic thermal motion of the Li(2) ions.

The number of Li(2) ions vibrating with large amplitudes in the direction of neighboring occupied Li(2) sites has increased such that now the Li(2)–Li(2) interaction results in an additional expansion of *a*.

The usual structure factor includes only harmonic thermal vibrations. Therefore, it cannot describe the strong anharmonic thermal vibrations and the corresponding electron density distribution of the Li(2) sites correctly. Likewise, corresponding least-squares programs adapt the usual structure parameters to an assumed harmonic distribution. This results in an overproportional decrease of the occupation probability and an overproportional increase of *u* ($\perp c$) of Li(2), whereas the defect concentration at the Li(2) positions has probably not changed, but only the number of highly excited Li(2) ions has increased.

The relations between anharmonic thermal vibrations and ionic conductivity described here have also been observed in AgI in a similar way (Cava, Reidinger & Wuensch, 1977).

We acknowledge many fruitful discussions with Professor A. Rabenau and Dr W. Weppner, Max-Planck-Institut für Festkörperforschung, Stuttgart, and with Professor R. A. Huggins, currently at the Max-Planck-Institut, Stuttgart, on sabbatical leave from Stanford University. We thank R. A. Huggins and W. Weppner for the careful and critical reading of the manuscript.

References

ALPEN, U. VON, BELL, M. F., WICHELHAUS, W., CHEUNG, K. Y. & DUDLEY, G. J. (1978). *Electrochim. Acta.* In the press.

ALPEN, U. VON, RABENAU, A. & TALAT, G. H. (1977). *Appl. Phys. Lett.* **30**, 621–623.

BOUKAMP, B.A. & HUGGINS, R. A. (1976). *Phys. Lett. A*, **58**, 231–233.

CAVA, R. J., REIDINGER, F. & WUENSCH, B. J. (1977). *Solid State Commun.* **24**, 411–416.

HONG, H. Y. P. (1978). *Mater. Res. Bull.* **13**, 117–124.

International Tables for X-ray Crystallography (1974). Vol. IV. Birmingham: Kynoch Press

LARSON, A. C. (1967). *Acta Cryst.* **23**, 664–665.

RABENAU, A. & SCHULZ, H. (1976). *J. Less-Common Met.* **50**, 155–159.

SCHÖNHERR, E., MÜLLER, G. & WINKLER, E. (1978). *J. Cryst. Growth*, **43**, 469–472.

SCHULZ, H. & SCHWARZ, K. H. (1978). *Acta Cryst.* A**34**, 999–1005.

SCHWARZ, K. H. & SCHULZ, H. (1978). *Acta Cryst.* A**34**, 994–999.

WAHL, J. & HOLLAND, U. (1978). *Solid State Commun.* **27**, 237–241.

ZINTL, E. & BRAUER, G. (1935). *Z. Elektrochem.* **41**, 102–107.

Acta Cryst. (1979). A**35**, 314–316

On the Choice of Elastic Constants in Evaluating Thermal Diffuse Scattering Corrections

BY G. DE WITH*

Chemical Physics Laboratory, Twente University of Technology, P.O. Box 217, *Enschede, The Netherlands*

(*Received* 5 *June* 1978; *accepted* 28 *September* 1978)

Abstract

The elastic stiffness constants for the calculation of the thermal diffuse scattering correction of X-ray reflexions should be the isothermal ones. However, adiabatic ones are mostly used. It is shown that, despite a relatively large difference between both types of elastic stiffness constants for pyrazine, the resulting thermal diffuse scattering correction is hardly affected.

At present thermal diffuse scattering (TDS) corrections of X-ray reflexions are usually evaluated in the so-called long-wave approximation. In this approximation the TDS correction factor α is given by (Cochran, 1969; Harada & Sakata, 1974)

$$\alpha = (2\pi)^{-3} \int_{\text{scan}} J(\mathbf{q})\, \mathrm{d}\mathbf{q},$$

with

$$J(\mathbf{q}) = \frac{k_B T}{q^2} \sum_{l,l} s_l (\mathbf{A}^{-1})_{jk} s_l$$

* Present address: Philips Research Laboratories, Eindhoven, The Netherlands.

0567-7394/79/020314-03$01.00